STRUCTURAL BIOLOGY COMMUNICATIONS

ISSN 2053-230X

Structural basis for the recognition of the scaffold protein Frmpd4/Preso1 by the TPR domain of the adaptor protein LGN

Hiroki Takayanagi, Satoru Yuzawa and Hideki Sumimoto*

Department of Biochemistry, Kyushu University Graduate School of Medical Sciences, 3-1-1 Maidashi, Higashi-ku, Fukuoka 812-8582, Japan. *Correspondence e-mail: hsumi@med.kyushu-u.ac.jp

Received 8 November 2014
Accepted 26 December 2014

Keywords: LGN; Frmpd4.

PDB references: LGN complexed with Frmpd4-L, 4wnd; LGN complexed with Frmpd4-S, 4wne; oxidized LGN complexed with Frmpd4, 4wnf

The adaptor protein LGN interacts *via* the N-terminal domain comprising eight tetratricopeptide-repeat (TPR) motifs with its partner proteins mInsc, NuMA, Frmpd1 and Frmpd4 in a mutually exclusive manner. Here, the crystal structure of the LGN TPR domain in complex with human Frmpd4 is described at 1.5 Å resolution. In the complex, the LGN-binding region of Frmpd4 (amino-acid residues 990–1011) adopts an extended structure that runs antiparallel to LGN along the concave surface of the superhelix formed by the TPR motifs. Comparison with the previously determined structures of the LGN–Frmpd1, LGN–mInsc and LGN–NuMA complexes reveals that these partner proteins interact with LGN TPR1–6 *via* a common core binding region with consensus sequence (E/Q)*X*E*X*$_{4–5}$(E/D/Q)*X*$_{1–2}$(K/R)*X*$_{0–1}$(V/I). In contrast to Frmpd1, Frmpd4 makes additional contacts with LGN *via* regions N- and C-terminal to the core sequence. The N-terminal extension is replaced by a specific α-helix in mInsc, which drastically increases the direct contacts with LGN TPR7/8, consistent with the higher affinity of mInsc for LGN. A crystal structure of Frmpd4-bound LGN in an oxidized form is also reported, although oxidation does not appear to strongly affect the interaction with Frmpd4.

1. Introduction

The adaptor protein LGN plays a crucial role in mitotic spindle orientation and cell polarization *via* interaction with multiple targets such as the nuclear mitotic apparatus protein NuMA and the cell-polarity protein mInsc (Du & Macara, 2004; Žigman *et al.*, 2005; Konno *et al.*, 2008; Kamakura *et al.*, 2013; Williams *et al.*, 2014). The N-terminal half of LGN comprises eight copies of a tetratricopeptide-repeat (TPR) motif, each adopting a helix–turn–helix structure of Aα and Bα, to form a right-handed superhelical domain (Yuzawa *et al.*, 2011; Zhu *et al.*, 2011), whereas the C-terminal half contains four GoLoco/GPR motifs, each capable of binding to GDP-bound Gαi (Willard *et al.*, 2004). The TPR domains of LGN and its related protein AGS3 directly interact with mInsc (Izaki *et al.*, 2006; Lechler & Fuchs, 2005; Žigman *et al.*, 2005), NuMA (Du & Macara, 2004) and the multidomain scaffold proteins Frmpd1 (An *et al.*, 2008; Yuzawa *et al.*, 2011) and Frmpd4 (also known as Preso1; Yuzawa *et al.*, 2011). Among the known LGN partners, mInsc has the highest affinity and thus can efficiently replace NuMA, Frmpd1 and Frmpd4 (Yuzawa *et al.*, 2011; Zhu *et al.*, 2011).

Human Frmpd4 comprised of 1322 amino acids contains WW, PDZ and FERM domains in the N-terminal region (see Fig. 1*a*) and interacts with LGN *via* a region in the C-terminal half which shows considerable similarity to part of the LGN-

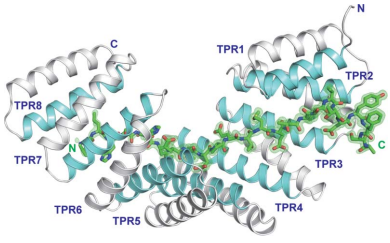

binding site in mInsc (Yuzawa *et al.*, 2011). Frmpd4 has been reported to modulate dendritic spine morphogenesis (Lee *et al.*, 2008) and to stabilize the interaction between the group I metabotropic glutamate receptors mGluR1/5 and the adaptor protein Homer, thereby attenuating calcium influx into spinal neurons (Hu *et al.*, 2012), although the role of the LGN–Frmpd4 interaction in these events remains to be elucidated. LGN binds to Frmpd4 with a higher affinity than that for Frmpd1 (Yuzawa *et al.*, 2011), a protein that has a similar domain architecture as Frmpd4 apart from the absence of the WW domain (An *et al.*, 2008). A crystal structure of the TPR domain of mouse LGN complexed with a human Frmpd1 fragment has recently been solved at 2.4 Å resolution (Pan *et al.*, 2013), which shows that complex formation is largely dependent on polar residues in the sequence (E/Q)*X*E$X_{4–5}$(E/D/Q)$X_{1–2}$(K/R) of the LGN partners.

Here, we report a crystal structure of the human LGN-TPR–human Frmpd4 complex determined at 1.5 Å resolution. In addition to the presently identified extended LGN-binding motif (E/Q)*X*E$X_{4–5}$(E/D/Q)$X_{1–2}$(K/R)$X_{0–1}$(V/I), Frmpd4 but not Frmpd1 uses its N- and C-terminal flanking regions for interaction with LGN, which appears to agree with a higher affinity of Frmpd4 than that of Frmpd1. Comparison with the previously determined LGN–mInsc complex reveals that Frmpd4 and mInsc similarly form extensive direct and water-mediated polar interactions *via* the core LGN-binding motif; on the other hand, tight contacts *via* the mInsc-specific α-helix (N-terminal to the core LGN-binding motif) are partially replaced by water molecules that bridge LGN and the N-terminal extension of Frmpd4, which may stabilize the interaction and/or improve the interface complementarity. In addition, we also describe a crystal structure of Frmpd4-bound LGN in an oxidized form.

2. Materials and methods

2.1. Protein expression and purification

The cDNAs for human LGN-N (amino-acid residues 13–414) and the human Frmpd4 fragment consisting of amino acids 978–1025 (Frmpd4-L) were cloned as described previously (Yuzawa *et al.*, 2011) and ligated into pGEX-6P (GE Healthcare) for expression as a glutathione *S*-transferase (GST)-fused protein or into modified pRSFDuet-1 (Novagen) for expression as a protein with an N-terminal hexahistidine (His) tag followed by a rhinovirus 3C protease cleavage site or

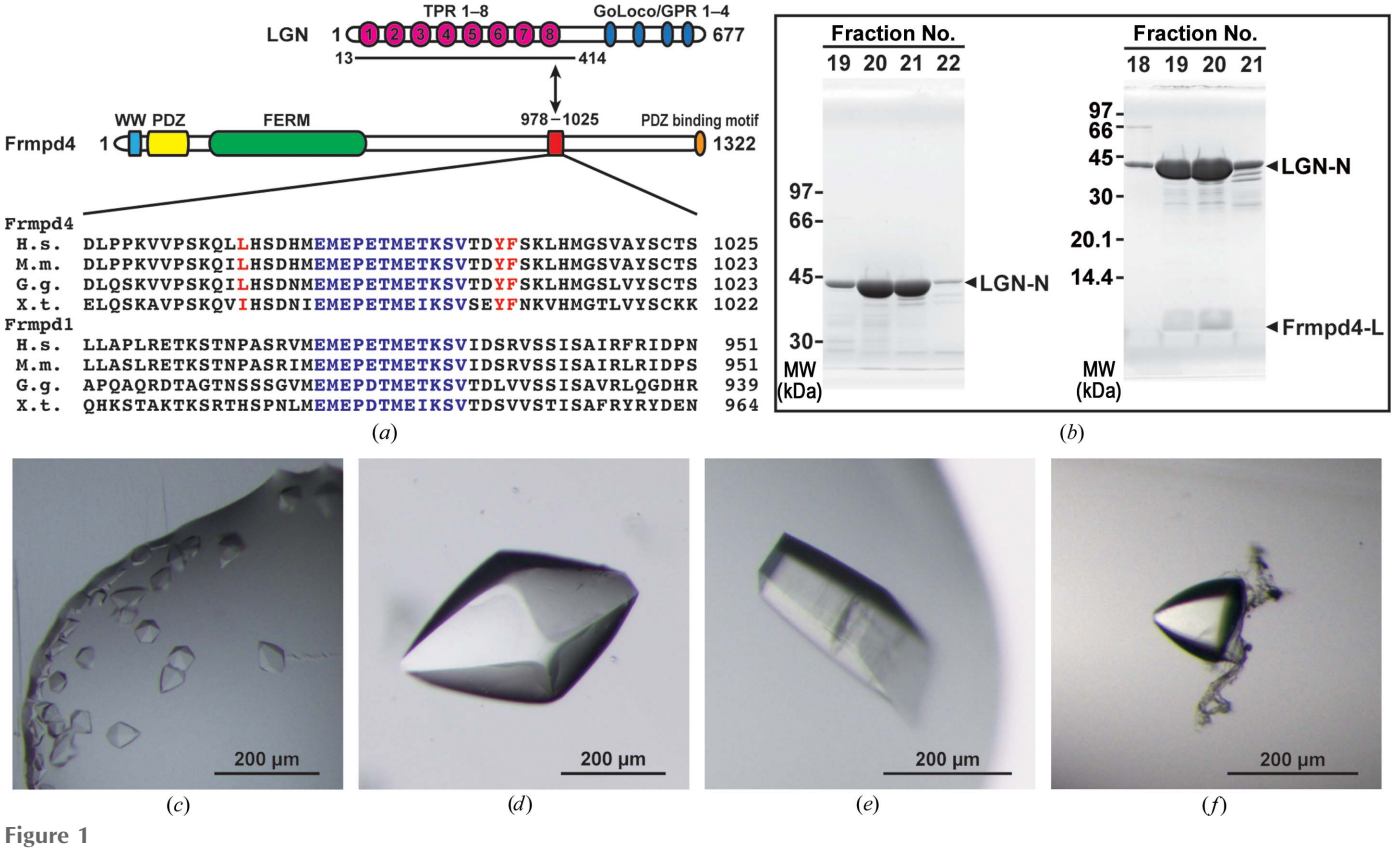

Figure 1
Purification and crystallization of the LGN–Frmpd4 complex. (*a*) The domain arrangements of human LGN and Frmpd4 are schematically represented. LGN-binding sites in the Frmpd proteins are aligned: *Homo sapiens* (H.s.), *Mus musculus* (M.m.), *Gallus gallus* (G.g.) and *Xenopus tropicalis* (X.t.). Residues in the core LGN-binding motif are shown in blue and residues that participate in binding to LGN but are located outside of the core are shown in red (see the text for details). (*b*) LGN-N (left) and LGN-N–Frmpd4-L (right) were applied onto a HiLoad 26/600 Superdex 200 column and 10 ml fractions were collected from the column and analyzed by SDS–PAGE with CBB staining. Positions of marker proteins are indicated in kDa. (*c*) Initial crystals of LGN-N–Frmpd4-S. (*d*) An optimized crystal of LGN-N–Frmpd4-S. (*e*) A crystal of LGN-N–Frmpd4-L. (*f*) A crystal of oxidized LGN-N in complex with Frmpd4-L.

Table 1
Crystallographic data-collection and refinement statistics.

Values in parentheses are for the outer shell.

	LGN-N–Frmpd4-S (PDB entry 4wne)	LGN-N–Frmpd4-L (PDB entry 4wnd)	Oxidized LGN-N–Frmpd4-L (PDB entry 4wnf)
Data collection and processing			
Diffraction source	BL1A, PF	BL44XU, SPring-8	BL44XU, SPring-8
Wavelength (Å)	1.1000	0.9000	0.9000
Temperature (K)	95	90	90
Detector	PILATUS 2M-F	Rayonix MX-300 HE	Rayonix MX-300 HE
Space group	$P6_122$	$P2_1$	$P6_122$
Unit-cell parameters (Å, °)	$a = b = 91.784$, $c = 176.783$, $\alpha = \beta = 90.000$, $\gamma = 120.000$	$a = 45.487$, $b = 64.786$, $c = 69.118$, $\alpha = \gamma = 90.000$, $\beta = 102.335$	$a = b = 92.599$, $c = 175.238$, $\alpha = \beta = 90.000$, $\gamma = 120.000$
Resolution range (Å)	50–2.00 (2.03–2.00)	50–1.50 (1.53–1.50)	50–2.90 (2.95–2.90)
Total No. of reflections	286743	379458	74336
No. of unique reflections	30371 (1484)	61319 (3013)	10385 (496)
Completeness (%)	99.2 (99.1)	98.8 (97.7)	99.3 (100)
Multiplicity	9.4 (9.6)	6.2 (5.0)	7.2 (7.6)
Mean $I/\sigma(I)$	20.2 (2.06)	36.5 (2.72)	18.2 (2.73)
R_{merge}	0.079 (0.881)	0.037 (0.446)	0.075 (0.502)
Refinement and validation			
Resolution used in refinement (Å)	39.78–2.00 (2.05–2.00)	46.79–1.50 (1.54–1.50)	39.12–2.90 (2.98–2.90)
No. of reflections, working set	28795 (2092)	58188 (4005)	9777 (692)
No. of reflections, test set	1533 (98)	3108 (193)	513 (47)
Final R_{work}	0.210 (0.277)	0.163 (0.242)	0.237 (0.316)
Final R_{free}	0.238 (0.327)	0.182 (0.267)	0.280 (0.350)
No. of non-H atoms			
Protein	2621	2962	2065
Ions	0	21	0
Ligands	0	69	0
Water	106	298	0
R.m.s.d., bond lengths (Å)	0.009	0.012	0.009
R.m.s.d., bond angles (°)	1.029	1.105	1.138
Mean B factor (Å^2)	51.0	24.1	88.3
Ramachandran plot			
Favoured regions (%)	95.8	96.6	95.5
Additionally allowed (%)	4.2	3.4	4.5
Outliers (%)	0	0	0

with an N-terminal maltose-binding protein (MBP) tag, a subsequent rhinovirus 3C protease cleavage site and a C-terminal His tag. All of the constructs were sequenced to confirm their identities. For preparation of the LGN-N–Frmpd4-S complex, bacterially expressed LGN-N was purified as described previously (Yuzawa *et al.*, 2011) and the purified protein was mixed with a chemically synthesized Frmpd4 fragment consisting of amino acids 987–1011 (Frmpd4-S). For preparation of the LGN-N–Frmpd4-L complex, *Escherichia coli* BL21(DE3) cells were doubly transformed with pRSFDuet-1 for His–LGN-N and pGEX-6P for GST–Frmpd4-L and the complex was subjected to purification using glutathione Sepharose 4B beads (GE Healthcare), cleavage with PreScission protease (GE Healthcare), removal of GST-containing proteins with a glutathione Sepharose 4B column and further purification by gel-filtration chromatography using a HiLoad 26/600 Superdex 200 column (GE Healthcare), as described previously (Yuzawa *et al.*, 2011).

2.2. Crystallization and data collection

The LGN-N–Frmpd4-S and LGN-N–Frmpd4-L complexes were dissolved in 50 m*M* NaCl, 2 m*M* tris(2-carboxyethyl)phosphine, 25 m*M* Tris–HCl pH 8.0 and used for crystallization at 293 K. Crystallization screening and optimization were performed as described previously (Yuzawa *et al.*, 2011). Small crystals of the LGN-N–Frmpd4-S complex were grown using condition No. 72 of The PACT Suite (Qiagen) and were subsequently crushed for microseeding (Luft & DeTitta, 1999). In combination with microseeding, the LGN-N–Frmpd4-S complex was crystallized by hanging-drop vapour diffusion against a reservoir solution consisting of 20%(*w*/*v*) PEG 3350, 0.2 *M* NaBr, 0.1 *M* bis-tris propane pH 7.25. The LGN-N–Frmpd4-L complex was crystallized by the microbatch-under-oil method (Chayen *et al.*, 1990): crystals were obtained using a 1:3 mixture of silicone and paraffin oils with drops consisting of 1 µl protein solution (7.5 mg ml^{-1}) and 1 µl precipitant solution (20% PEG 3350, 0.2 *M* KSCN, 0.1 *M* bis-tris propane pH 7.5). Crystals of oxidized LGN-N in complex with Frmpd4-L were obtained after 15 months incubation using the sitting-drop vapour-diffusion method by mixing equal volumes of protein solution and reservoir solution (condition No. 76 from The PACT Suite). The crystals of the LGN-N–Frmpd4-S complex and the LGN-N–Frmpd4-L complex were cryoprotected by soaking in linear perfluoropolyether MW 2700 (Alfa Aesar) or in mother liquor supplemented with 15 or 20%(*v*/*v*) ethylene glycol, respectively, and were subsequently flash-cooled in liquid nitrogen. X-ray diffraction data were collected using ADSC Quantum 270 and PILATUS 2M-F detectors installed on beamline

BL1A at the Photon Factory (PF), KEK, Tsukuba, Japan and using a Rayonix MX-300HE detector installed on beamline BL44XU at SPring-8, Harima, Japan and were integrated and scaled using *HKL*-2000 (Otwinowski & Minor, 1997).

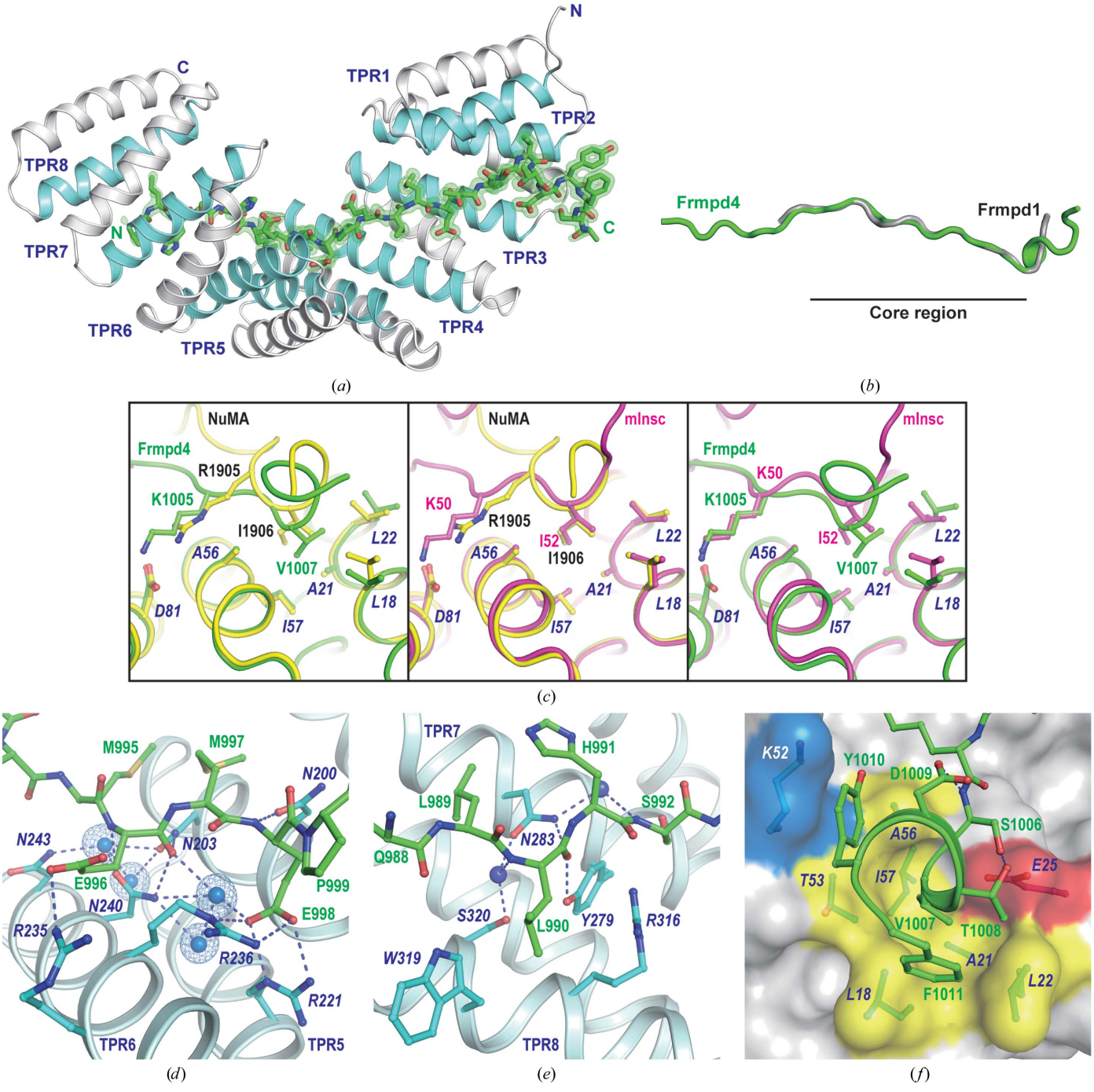

Figure 2
Structure of the LGN–Frmpd4 complex. (*a*) The TPR motifs in LGN-N are illustrated as a cartoon model. The Aα and Bα helices are coloured cyan and grey, respectively. The LGN-binding region of Frmpd4 is shown as a green stick model with a $2F_o - F_c$ electron-density map contoured at 1σ. (*b*) The structure of the Frmpd1 fragment in the LGN–Frmpd1 complex (PDB entry 4g2v) is superimposed on that of the Frmpd4 fragment in the LGN–Frmpd4 complex. Ribbon diagrams of Frmpd4 and Frmpd1 are coloured green and grey, respectively. The common core LGN-binding region is indicated. (*c*) Enlarged views of the complex of LGN with a fragment containing the conserved valine/isoleucine in the core LGN-binding region. The regions of Frmpd4, NuMA and mInsc in their respective LGN complexes are coloured green, yellow and magenta, respectively. (*d*) Polar interactions between the core region of Frmpd4 and LGN are shown as dashed lines using a cutoff of 3.5 Å. Residues in Frmpd4 and LGN are labelled in green and blue, respectively. Spheres indicate water molecules with electron density contoured at 1σ. (*e*) Polar interactions of LGN with an Frmpd4 fragment N-terminal to the core binding region are shown as dashed lines. (*f*) Surface representation of the binding interface of LGN with an Frmpd4 fragment C-terminal to the core binding region. The hydrophobic, acidic and basic residues of LGN are coloured yellow, red and blue, respectively.

2.3. Structure determination and refinement

The structure of the LGN-N–Frmpd4-S complex was solved by molecular replacement using *MOLREP* (Vagin & Teplyakov, 2010) with the LGN TPR domain complexed with mInsc as the search model (PDB entry 3sf4; Yuzawa *et al.*, 2011). Iterative model building and refinement were performed using *Coot* (Emsley *et al.*, 2010) and *REFMAC*5 (Murshudov *et al.*, 2011). The structures of the LGN-N–Frmpd4-L complexes were determined by molecular replacement using the LGN-N–Frmpd4-S coordinates. Atomic coordinates and structure factors have been deposited in the PDB as entries 4wnd (LGN-N–Frmpd4-L), 4wne (LGN-N–Frmpd4-S) and 4wnf (oxidized LGN-N–Frmpd4-L). Data-collection and refinement statistics are shown in Table 1. Interaction areas were calculated using *PISA* (Krissinel & Henrick, 2007). Pairwise structural comparisons were performed using LSQ superpose in *Coot*. Structure figures were prepared using the program *PyMOL* (http://www.pymol.org/).

2.4. Isothermal titration calorimetry

Complex formation between LGN and Frmpd4 was measured by isothermal titration calorimetry (ITC) using a MicroCal VP-ITC calorimeter (MicroCal Inc.; Islam *et al.*, 2012). Bacterially expressed wild-type (wt) MBP–Frmpd4-(978–1011) or a mutant protein with the L990A/Y1010A/F1011A substitution was purified with Amylose Resin (New England Biolabs) followed by gel-filtration chromatography. All proteins were dialyzed against ITC buffer [150 m*M* NaCl, 1 m*M* tris(2-carboxyethyl)phosphine, 25 m*M* sodium phosphate pH 7.0] and experiments were performed at 298 K. The titration cell was loaded with 5 µ*M* LGN-N, and one 5 µl injection and 24 subsequent 10 µl injections of 50 µ*M* MBP–Frmpd4-(978–1011) (wt) or MBP–Frmpd4-(978–1011) (L990A/Y1010A/F1011A) were administrated at 240 s intervals. Heats of dilution were determined by titrating MBP–Frmpd4 into the ITC buffer and were subtracted from the raw titration data prior to analysis using the *Origin* v.7.0 evaluation software, assuming a single-site binding model.

2.5. MBP pull-down binding assay

Bacterially expressed MBP–Frmpd4-L–His was purified with COSMOGEL His-Accept (Nacalai Tesque) as described previously (Yuzawa *et al.*, 2011). LGN-N (0.25 µ*M*) and MBP–Frmpd4-L–His or MBP alone (0.5 µ*M*) were incubated for 15 min at 277 K with dithiothreitol (5.0 m*M*) or H_2O_2 (0.5 or 1.0 m*M*) in 250 µl of a buffer consisting of 150 m*M* NaCl, 0.002% Triton X-100, 20 m*M* HEPES pH 7.4. Proteins were pulled down with Amylose Resin and subjected to SDS–PAGE followed by staining with Coomassie Brilliant Blue (CBB).

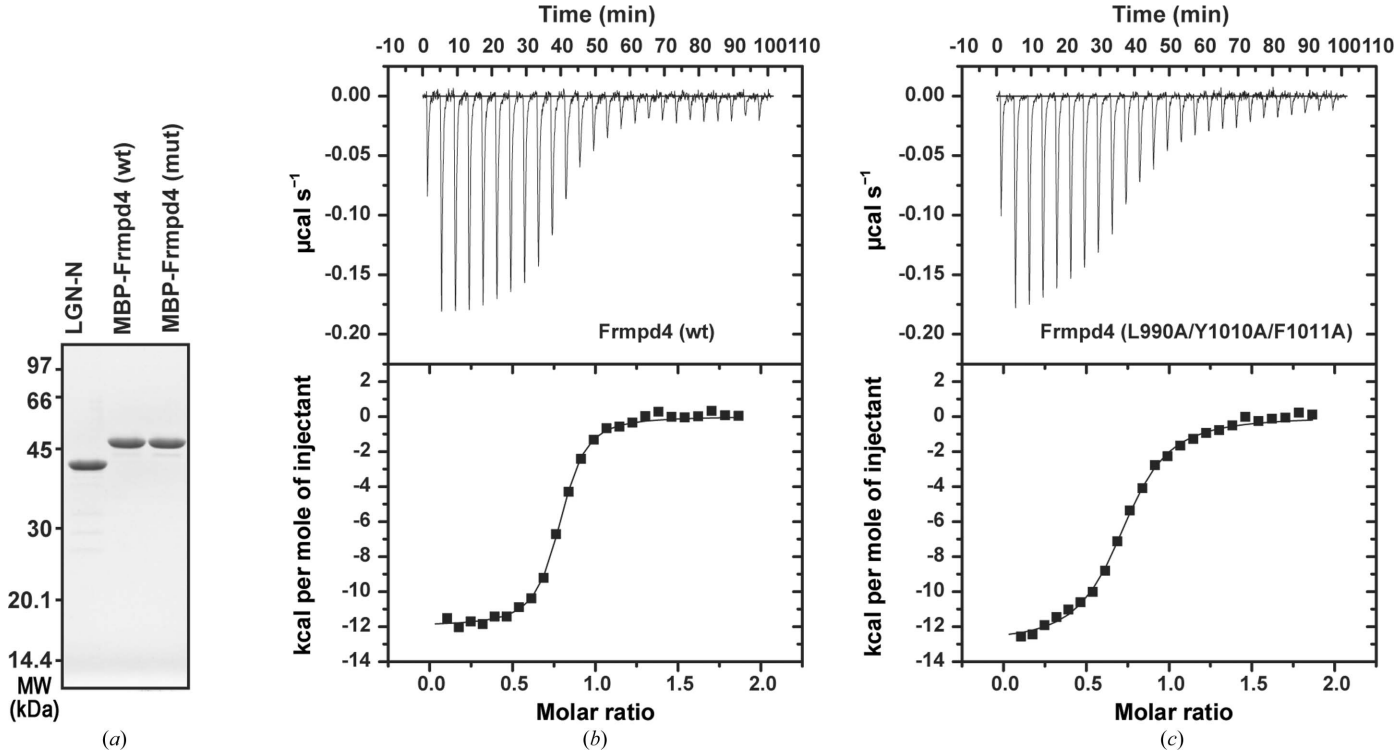

Figure 3
ITC measurements of complex formation between LGN and Frmpd4. (*a*) SDS–PAGE analysis of purified proteins that were used in ITC measurements. LGN-N, wild-type (wt) MBP–Frmpd4-(978–1011) and mutant (mut) MBP–Frmpd4-(978–1011) with the L990A/Y1010A/F1011A substitution were subjected to SDS–PAGE followed by staining with CBB. Positions of marker proteins are indicated in kDa. In ITC analysis, the upper part shows the raw calorimetric data for the interaction of LGN-N with MBP–Frmpd4-(978–1011) (wt) (*b*) or MBP–Frmpd4-(978–1011) (L990A/Y1010A/F1011A) (*c*) and the lower part shows the integrated heat changes corrected for heat of dilution and fitted to a single-site binding model.

3. Results and discussion

3.1. Structure of the LGN TPR domain in complex with Frmpd4

We prepared a crystal of LGN-N (residues 13–414) in complex with Frmpd4-L (residues 978–1025; Fig. 1) and determined its structure at 1.5 Å resolution (Fig. 2*a*). In the complex, the Frmpd4 segment of residues 990–1011 adopts an extended structure with a C-terminal short 3_{10}-helix (residues 1007–1009) and runs along a concave channel of the superhelix formed by the eight TPR motifs of LGN in an antiparallel manner (Fig. 2*b*), burying 3482 Å^2 of the total surface area. This area is larger than that of the LGN–Frmpd1 complex (2541 Å^2) solved at 2.4 Å resolution (Pan *et al.*, 2013), which is consistent with the previous finding that the TPR domain of LGN binds to Frmpd4 with a higher affinity than that for Frmpd1 (Yuzawa *et al.*, 2011).

Pan *et al.* (2013) recently proposed the sequence (E/Q)*X*-E$X_{4–5}$(E/D/Q)$X_{1–2}$(K/R) as the common motif for binding to TPR2–6 in LGN on the basis of the structures of LGN complexed with Frmpd1, mInsc and NuMA. In addition to the corresponding region of Frmpd4 (residues **E**M**E**PETM**E**T**K**, residues 996–1005), the invariant valine that is located two residues C-terminal to the region (Val1007 in Frmpd4; Fig. 1*a*) fits into a hydrophobic pocket formed by Leu18, Ala21, Leu22, Thr53, Ala56 and Ile57 in LGN. It should be noted that not only the corresponding residues in the LGN-binding regions of mInsc (Ile52) and its *Drosophila* homologue (Ile334) (Yuzawa *et al.*, 2011; Culurgioni *et al.*, 2011) but also that in NuMA (Ile1906) are buried in the same hydrophobic pocket (Fig. 2*c*). Therefore, we designate the sequence (E/Q)*X*E$X_{4–5}$(E/D/Q)$X_{1–2}$(K/R)$X_{0–1}$(V/I) as the core LGN-binding motif; the motif is completely conserved between Frmpd1 and Frmpd4 during evolution (Fig. 1*a*). The conserved polar residues in Frmpd4 play crucial roles in interaction with LGN *via* hydrogen bonds and salt bridges, as observed in the LGN–Frmpd1 complex (Pan *et al.*, 2013): some of the interactions are shown in Fig. 2(*d*).

3.2. Role of the regions N- and C-terminal to the core LGN-binding motif in Frmpd4

In contrast to Frmpd1, which binds to LGN almost exclusively *via* the core motif region (Pan *et al.*, 2013), Frmpd4 makes multiple additional contacts with LGN *via* extensions N- and C-terminal to the core (Fig. 2*b*). On the other hand, the amino-acid sequences of the corresponding regions are divergent in Frmpd1. Leu990, a conserved residue that is located N-terminal to the core LGN-binding motif (Fig. 1*a*), forms hydrogen bonds *via* the main chain to the side chains of Asn283 and Tyr279 in LGN TPR7, whereas the side chain of Leu990 fits into the groove formed by Arg316 and Trp319 in LGN TPR8 (Fig. 2*e*). Because a region C-terminal to the core LGN-binding region in the LGN-N–Frmpd4-L complex makes contacts with a neighbouring LGN-N, we determined another LGN-N–Frmpd4 complex structure in a different crystal form (namely the LGN-N–Frmpd4-S complex; Fig. 1 and Table 1) to exclude the possibility of a crystal-packing artifact. In the complex, Frmpd4-S adopts a structure similar to that of LGN-N-bound Frmpd4-L, with the C-terminal region forming a short 3_{10}-helix, but makes little crystal-packing interaction with the neighbouring LGN-N molecule. Tyr1010 in Frmpd4 makes direct contacts with the side chain of Lys52 in LGN TPR2, whereas the side chain of Phe1011 fits into a hydrophobic pocket containing Leu18, Ala21 and Leu22 in LGN TPR1 (Fig. 2*f*). Both Tyr1010 and Phe1011 are evolutionarily conserved in Frmpd4 but are replaced by various residues in Frmpd1 (Fig. 1*a*). Thus, the N- and C-terminal flanking regions in Frmpd4 directly interact with TPR7/8 and TPR1/2, respectively, and thus appear to provide a higher affinity for LGN than that of Frmpd1.

To further clarify the functional role of the regions N- and C-terminal to the core LGN-binding motif in Frmpd4, we introduced alanine substitutions for the three invariant residues Leu990, Tyr1010 and Phe1011, all of which make direct contacts with the LGN TPR domain (Fig. 2), and estimated the affinities for LGN of wild-type Frmpd4 and a mutant protein carrying the L990A/Y1010A/F1011A substitution by

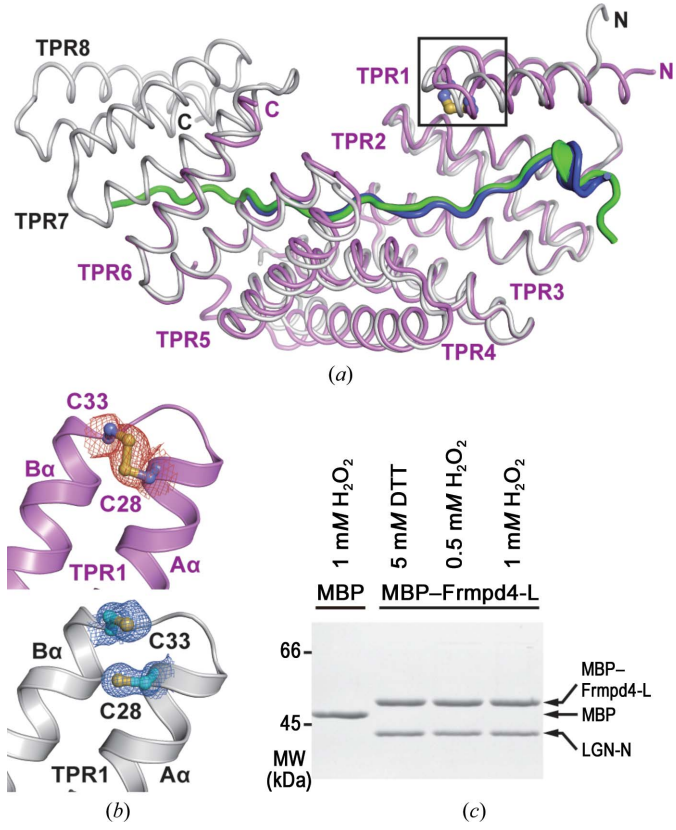

Figure 4
Structure of oxidized LGN in complex with Frmpd4. (*a*) Superposition of the structure of Frmpd4-L-bound LGN-N in an oxidized form with that of the LGN-N–Frmpd4-L complex. Frmpd4 and LGN in the oxidized complex are coloured blue and violet, respectively; Frmpd4 and LGN in the reduced complex are shown in green and grey, respectively. (*b*) Enlarged views of LGN TPR1 in the oxidized (upper) and reduced (lower) forms. Cys28 and Cys33 are shown as ball-and-stick models with electron density contoured at 1σ. (*c*) Interaction of LGN with Frmpd4 under reduced and oxidized conditions. LGN-N binding to MBP–Frmpd4-L in the presence of dithiothreitol (DTT) or H_2O_2 was estimated by the MBP pull-down assay.

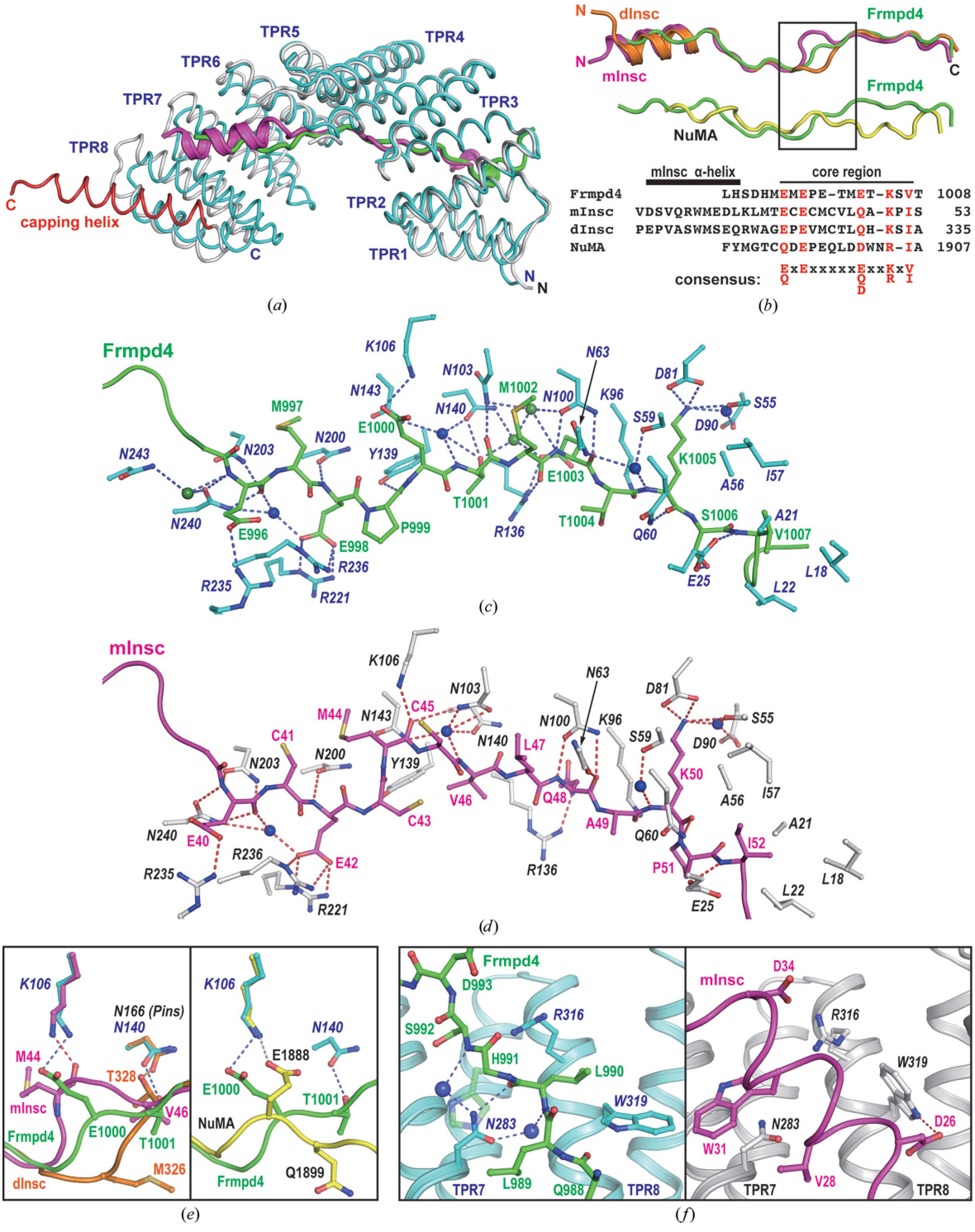

Figure 5
Recognition of various partner proteins by the LGN TPR domain. (*a*) Superposition of the LGN–mInsc complex (PDB entry 3sf4) with the LGN–Frmpd4 complex. LGN and Frmpd4 in the LGN–Frmpd4 complex are coloured cyan and green, respectively. In the LGN–mInsc complex, mInsc (residues 23–58) is shown in magenta, whereas the TPR domain and the capping helix of LGN are coloured grey and red, respectively. (*b*) The structure of Frmpd4 in the LGN–Frmpd4 complex is superimposed on those of mInsc (PDB entry 3sf4), NuMA (PDB entry 3ro2; Zhu *et al.*, 2011) and dInsc (PDB entry 4a1s; Culurgioni *et al.*, 2011) in their respective LGN complexes. The core LGN-binding region and its N-terminal extension in Frmpd4 (green), mInsc (magenta), dInsc (orange) and NuMA (yellow) are shown as ribbon diagrams. The amino-acid sequences of Frmpd4, mInsc, dInsc and NuMA are aligned. (*c*) Interactions involved in LGN binding to the core region of Frmpd4. Key residues are shown as stick models coloured green (residues 996–1007 in Frmpd4) and cyan (LGN). (*d*) Interactions involved in LGN binding to mInsc. Key residues are shown as stick models coloured magenta (residues 40–52 in mInsc) and grey (LGN). (*e*) Enlarged views of the LGN partner fragments boxed in (*b*). The regions of Frmpd4, mInsc, dInc and NuMA in their respective LGN (or Pins for dInsc) complexes are coloured green, magenta, orange and yellow, respectively. The side chains of key residues and the main chain of Met44 in mInsc are shown as stick models. (*f*) Enlarged views of the complex of LGN TPR7/8 with an extension N-terminal to the core LGN-binding region of Frmpd4 (left) and mInsc (right).

isothermal titration calorimetry (ITC). As shown in Fig. 3, wild-type Frmpd4 interacted with LGN-N with an apparent K_d of 32.9 ± 7.8 n*M* (*n* = 3), whereas the mutant protein bound with a K_d of 191 ± 43 n*M* (*n* = 3). Thus, the L990A/Y1010A/F1011A substitution resulted in a significant decrease in the affinity for LGN ($P < 0.01$; Student's *t* test), confirming that the flanking regions in Frmpd4 participate in binding to LGN.

3.3. The effect of LGN TPR domain oxidation on its interaction with Frmpd4

In TPR1 of LGN, the S atom of the evolutionarily conserved residue Cys28 in TPR1Aα is located very close to that of the invariant residue Cys33 in TPR1Bα (Fig. 4*a*). After the LGN-N–Frmpd4-L complex was incubated under crystallization conditions for 15 months, we obtained by chance a crystal of Frmpd4-bound LGN-N that harbours a spontaneously formed disulfide bond between Cys28 and Cys33 (Fig. 1) and determined its structure at 2.9 Å resolution (Fig. 4*a* and Table 1). Comparison of this structure with that of the reduced LGN-N in complex with the Frmpd4 fragment suggests that both the structure of the LGN TPR domain and its interaction interface with Frmpd4 are not strongly affected by the formation of the disulfide bond (Fig. 4*b*). Consistent with this, oxidation of the LGN TPR domain with hydrogen peroxide did not impair its interaction with the Frmpd4 fragment, as demonstrated by an MBP pull-down binding assay (Fig. 4*c*). Thus, formation of an intramolecular Cys28–Cys33 disulfide bond does not seem to function as a redox-dependent conformational switch in LGN.

3.4. Recognition of various partners by the LGN TPR domain

To clarify the difference in LGN recognition between Frmpd4 and mInsc, we compared the structure of the Frmpd4-bound LGN with that of the same region of LGN complexed with mInsc (Figs. 5*a*). Apart from the capping helix next to TPR8, which is visible in the LGN–mInsc complex (Yuzawa *et al.*, 2011) but not in the LGN–Frmpd4 complex (Fig. 5*a*), they share a similar TPR structure, with r.m.s.d.s of 0.87 Å for TPR2–6 (204 C^{α} atoms) and 2.38 Å for TPR1–8 (320 C^{α} atoms). The LGN-binding region of mInsc (residues 23–69) contains the N-terminal α-helix (residues 26–35) and the following extended region (Yuzawa *et al.*, 2011), the latter of which contains the sequence ECECMCVLQAKPI (residues 40–52) corresponding to the common LGN-binding motif (E/Q)*X*EX_{4-5}(E/D/Q)X_{1-2}(K/R)X_{0-1}(V/I) (Fig. 5*b*). The core regions of Frmpd4 and mInsc interact with LGN *via* extensive hydrogen bonds and salt bridges formed by the conserved polar residues (Glu996, Glu998, Glu1003 and Lys1005 in Frmpd4) and also *via* V/I-mediated hydrophobic interaction (Figs. 5*c* and 5*d*), burying total surface areas of 2255 $Å^2$ (Frmpd4) and 2199 $Å^2$ (mInsc) (Fig. 5*d*). The same interactions occur in the complex of the *Drosophila* LGN homologue Pins with *Drosophila* Inscuteable (dInsc; Culurgioni *et al.*, 2011). Furthermore, the present high-resolution structure of the LGN–Frmpd4 complex reveals that seven water molecules bound in the interface act as a bridge between LGN and the core binding region of Frmpd4 *via* hydrogen bonds (Fig. 5*c*); the majority of them also function in the LGN–mInsc complex (Fig. 5*d*) and in the Pins–dInsc complex (data not shown). It is known that water molecules can stabilize the complex between a protein and its ligand by hydrogen bonding to the two components and can also sculpt the protein surface to improve interface complementarity (Barillari *et al.*, 2007; Meenan *et al.*, 2010).

Among the LGN partners, the major difference in the core binding region exists in the dipeptide Glu1000-Thr1001 in Frmpd4, which is replaced by the tripeptide MC(V/T) in mInsc and dInsc and by the tripeptide EQL in NuMA (Fig. 5*b*). The side chains of Glu1000 and Thr1001 in Frmpd4 form a hydrogen bond to those of $Lys106_{LGN}$ and $Asn140_{LGN}$, respectively (Fig. 5*e*). NuMA also makes the former hydrogen bond but not the latter, but the opposite occurs in the case of dInsc (Fig. 5*e*). On the other hand, the main chain of mInsc interacts *via* a hydrogen bond with the side chain of $Lys106_{LGN}$ (Fig. 5*e*). Thus, in spite of the difference in the structure of this stretch, the partners appear to effectively interact with LGN. Taking together with the above-described importance of the conserved residues, (E/Q)*X*EX_{4-5}(E/D/Q)X_{1-2}(K/R)X_{0-1}(V/I) is likely to function as the common LGN-binding motif.

The high affinity of mInsc for LGN is owing to the Insc-specific α-helix that is located N-terminal to the common core LGN-binding region. Indeed, for instance, the invariant residues Val28 and Trp31 tightly sandwich the side chain of Asn283 in LGN TPR7 *via* multiple van der Waals contacts, whereas the side chains of Asp26 and Asp34 on the opposite side of the α-helix make a hydrogen bond to Trp319 and a salt bridge to Arg316 in LGN TPR8, respectively (Fig. 5*f*). These interactions are not observed in the complex of LGN with the weaker ligand Frmpd4. Instead, however, Asn283 in LGN TPR8 interacts with the main chain of Frmpd4 *via* direct and water-mediated hydrogen bonds (Fig. 5*f*). The bound waters are likely to play a role not only in stabilizing the LGN–Frmpd4 complex but also in improving interface complementarity.

Here, we carefully compare the present structure of the LGN–Frmpd4 complex with those of LGN bound to its other partners to identify the sequence (E/Q)*X*EX_{4-5}(E/D/Q)X_{1-2}(K/R)X_{0-1}(V/I) as the common core motif for binding to the versatile adaptor protein LGN. The regions N- and C-terminal to the core in Frmpd4 make additional contacts with LGN which specifically reinforce the interaction.

Acknowledgements

This work was supported in part by a Grant-in-Aid for Scientific Research on Innovative Areas 'Oxygen Biology: a new criterion for integrated understanding of life' (No. 26111009), and a KAKENHI Grant (No. 26440033) from MEXT (The Ministry of Education, Culture, Sports, Science and Technology, Japan) and by The Uehara Memorial Foundation. We thank Drs Atsushi Shimada (Kyushu University) and Daisuke Kohda (Kyushu University) for helpful advice, Yohko Kage (Kyushu University) and Namiko Kubo (Kyushu University) for technical assistance, Shoko Miura (Kyushu

University) for secretarial assistance, the beamline staff for technical support during data collection on the BL1A beamline at the Photon Factory and on the BL44XU beamline at SPring-8, and the technical staff of The Research Support Center, Research Center for Human Disease Modeling, Kyushu University Graduate School of Medical Sciences, Fukuoka, Japan.

References

An, N., Blumer, J. B., Bernard, M. L. & Lanier, S. M. (2008). *J. Biol. Chem.* **283**, 24718–24728.
Barillari, C., Taylor, J., Viner, R. & Essex, J. W. (2007). *J. Am. Chem. Soc.* **129**, 2577–2587.
Chayen, N. E., Shaw Stewart, P. D., Maeder, D. L. & Blow, D. M. (1990). *J. Appl. Cryst.* **23**, 297–302.
Culurgioni, S., Alfieri, A., Pendolino, V., Laddomada, F. & Mapelli, M. (2011). *Proc. Natl Acad. Sci. USA*, **108**, 20998–21003.
Du, Q. & Macara, I. G. (2004). *Cell*, **119**, 503–516.
Emsley, P., Lohkamp, B., Scott, W. G. & Cowtan, K. (2010). *Acta Cryst.* D**66**, 486–501.
Hu, J.-H., Yang, L., Kammermeier, P. J., Moore, C. G., Brakeman, P. R., Tu, J., Yu, S., Petralia, R. S., Li, Z., Zhang, P.-W., Park, J. M., Dong, X., Xiao, B. & Worley, P. F. (2012). *Nature Neurosci.* **15**, 836–844.
Islam, M. R., Nishie, M., Nagao, J., Zendo, T., Keller, S., Nakayama, J., Kohda, D., Sahl, H.-G. & Sonomoto, K. (2012). *J. Am. Chem. Soc.* **134**, 3687–3690.
Izaki, T., Kamakura, S., Kohjima, M. & Sumimoto, H. (2006). *Biochem. Biophys. Res. Commun.* **341**, 1001–1006.
Kamakura, S., Nomura, M., Hayase, J., Iwakiri, Y., Nishikimi, A., Takayanagi, R., Fukui, Y. & Sumimoto, H. (2013). *Dev. Cell*, **26**, 292–302.
Konno, D., Shioi, G., Shitamukai, A., Mori, A., Kiyonari, H., Miyata, T. & Matsuzaki, F. (2008). *Nature Cell Biol.* **10**, 93–101.
Krissinel, E. & Henrick, K. (2007). *J. Mol. Biol.* **372**, 774–797.
Lechler, T. & Fuchs, E. (2005). *Nature (London)*, **437**, 275–280.
Lee, H. W., Choi, J., Shin, H., Kim, K., Yang, J., Na, M., Choi, S. Y., Kang, G. B., Eom, S. H., Kim, H. & Kim, E. (2008). *J. Neurosci.* **28**, 14546–14556.
Luft, J. R. & DeTitta, G. T. (1999). *Acta Cryst.* D**55**, 988–993.
Meenan, N. A. G., Sharma, A., Fleishman, S. J., MacDonald, C. J., Morel, B., Boetzel, R., Moore, G. R., Baker, D. & Kleanthous, C. (2010). *Proc. Natl Acad. Sci. USA*, **107**, 10080–10085.
Murshudov, G. N., Skubák, P., Lebedev, A. A., Pannu, N. S., Steiner, R. A., Nicholls, R. A., Winn, M. D., Long, F. & Vagin, A. A. (2011). *Acta Cryst.* D**67**, 355–367.
Otwinowski, Z. & Minor, W. (1997). *Methods Enzymol.* **276**, 307–326.
Pan, Z., Shang, Y., Jia, M., Zhang, L., Xia, C., Zhang, M., Wang, W. & Wen, W. (2013). *J. Mol. Biol.* **425**, 1039–1049.
Vagin, A. & Teplyakov, A. (2010). *Acta Cryst.* D**66**, 22–25.
Willard, F. S., Kimple, R. J. & Siderovski, D. P. (2004). *Annu. Rev. Biochem.* **73**, 925–951.
Williams, S. E., Ratliff, L. A., Postiglione, M. P., Knoblich, J. A. & Fuchs, E. (2014). *Nature Cell Biol.* **16**, 758–769.
Yuzawa, S., Kamakura, S., Iwakiri, Y., Hayase, J. & Sumimoto, H. (2011). *Proc. Natl Acad. Sci. USA*, **108**, 19210–19215.
Zhu, J., Wen, W., Zheng, Z., Shang, Y., Wei, Z., Xiao, Z., Pan, Z., Du, Q., Wang, W. & Zhang, M. (2011). *Mol. Cell*, **43**, 418–431.
Žigman, M., Cayouette, M., Charalambous, C., Schleiffer, A., Hoeller, O., Dunican, D., McCudden, C. R., Firnberg, N., Barres, B. A., Siderovski, D. P. & Knoblich, J. A. (2005). *Neuron*, **48**, 539–545.